Nano Materials Science xxx (xxxx) xxx

Contents lists available at ScienceDirect

Nano Materials Science

journal homepage: www.keaipublishing.com/cn/journals/nano-materials-science/

MXene multi-functionalization of polyrotaxane based PCMs and the applications in electronic devices thermal management

Guang-Zhong Yin [a,b,*], Alba Marta López [b], Ignacio Collado [c], Antonio Vázquez-López [b,c], Xiang Ao [b], Jose Hobson [b,d], Silvia G. Prolongo [c,e], De-Yi Wang [a,b,**]

[a] Escuela Politécnica Superior, Universidad Francisco de Vitoria, Ctra. Pozuelo-Majadahonda Km 1.800, 28223 Pozuelo de Alarcón, Madrid, Spain
[b] IMDEA Materials Institute, C/Eric Kandel, 2, 28906, Getafe, Madrid, Spain
[c] Materials Science and Engineering Area, Escuela Superior de Ciencias Experimentales y Tecnología, Universidad Rey Juan Carlos, C/Tulipán s/n, 28933, Madrid, Spain
[d] Universidad Carlos III de Madrid, Departamento de Ciencia e Ingeniería de Materiales e Ingeniería Química, IAAB. Avda. Universidad, 30, 28911, Leganés, Madrid, Spain
[e] Instituto de Tecnologías para la Sostenibilidad, Universidad Rey Juan Carlos, C/Tulipán s/n, 28933, Madrid, Spain

ARTICLE INFO

Keywords:
Phase change materials
Thermal regulation
MXene
Polyrotaxane
Nanocomposites

ABSTRACT

The aim of this work was to improve the thermal conductivity and electromagnetic shielding of the leakage proof phase change materials (PCMs), in which a polyrotaxane (PLR) was used as a support material to encapsulate PEG 1k or PEG 6k and MXene as multi-functional filler. The PCMs can be processed conveniently by a hot press and the PEG 1k containing samples showed excellent flexibility. We conducted a systematic evaluation of the phase transition behavior of the material, thermal conductivity and electromagnetic shielding performance tests. Notably, the PCMs achieved a high enthalpy values (123.9–159.6 J/g). The PCMs exhibited an increase of 44.3 %, and 137.5 % in thermal conductivity values with higher MXene content (5 wt%) for PLR-PEG6k and PLR-PEG1k, respectively, and show high shape stability and no leakage during and after phase transition. The introduction of MXene can significantly improve the electromagnetic shielding performance of PCM composites. Typically, higher conductive samples (samples which contain high MXene contents) offer a higher EMI SE shielding, reaching a maximum of 4.67 dB at 5.6 GHz for PLR-1K-MX5. These improvements solve the main problems of organic PEG based PCMs, thus making PLR-PEG-MXene based PCMs good candidates for thermoregulators of both solid-state disks and smart phone. It is worth pointing out that the sample PLR-1k-MX5 can decrease 4.3 °C of the reference temperature during cellphone running. Moreover, the temperature of the protecting sheet in the simulated solid state disk with PCM was significantly lower (showing a decreasing of 7.9 °C) compared with the blank sample.

1. Introduction

The 5G era is gradually approaching, with the introduction of high frequency, the upgrade of hardware components, and the exponential increase in the number of networked devices and antennas, electromagnetic interference between devices and within the device itself is ubiquitous, and electromagnetic interference and electromagnetic radiation are harmful to electronic devices. At the same time, with the updating and upgrading of electronic products, the power consumption of the equipment continues to increase, and the calorific value also rises rapidly. The bottleneck of high-frequency and high-power electronic products in the future is the electromagnetic radiation and generated heat. To solve these problems, more and more electromagnetic shielding and heat-treatment strategies were added to the design of electronic products. Therefore, the role of electromagnetic shielding and heat dissipation materials and devices will become more and more important, and the demand will continue to grow in the future [1].

Phase Change Materials (PCMs) are notable for their capacity to store energy as latent heat and release it in response to environmental temperature variations [2]. They are widely utilized in applications such as temperature-adaptable greenhouses [3], solar energy storage [4], smartphone thermal regulation [5], and solar thermoelectric generators

* Corresponding author. Escuela Politécnica Superior, Universidad Francisco de Vitoria, Ctra. Pozuelo-Majadahonda Km 1.800, 28223 Pozuelo de Alarcón, Madrid, Spain.
** Corresponding author. Escuela Politécnica Superior, Universidad Francisco de Vitoria, Ctra. Pozuelo-Majadahonda Km 1.800, 28223 Pozuelo de Alarcón, Madrid, Spain.
E-mail addresses: amos.guangzhong@ufv.es (G.-Z. Yin), deyi.wang@imdea.org (D.-Y. Wang).

https://doi.org/10.1016/j.nanoms.2023.12.004

Available online xxxx

[6]. [7] PCMs face challenges like low thermal conductivity, poor form stability, and substance leakage during phase change, leading to operational failures [8]. Additionally, the difficulty of obtaining flexible PCM materials hinders practical applications, with many prepared materials being rigid or in powder form, necessitating secondary processing [9,10]. [11].

Polyethylene glycol (PEG)-based PCMs, a common example, find extensive use in solar energy [12], waste heat recovery [13], and electric energy storage [14] due to properties such as substantial phase transition enthalpy, a wide transition temperature range, and thermal and chemical stability [15]. However, like other organic PCMs, they encounter similar drawbacks, necessitating ongoing research and development to address these limitations and enhance the overall performance and versatility of PCM technology. At present, the research on the modification and application of PEG anti-leakage and thermal conductivity is in-depth and extensive [16,17]. In our previous studies [11,18], polyrotaxane (PLR) was proved to be an ideal support material for PEG for leakage proof and form stable PCMs, because it has the same main chain chemical structure as PEG work substance [19].

As mentioned before, smartphones continue to innovate and develop in the direction of thinner, lighter, integrated, and device miniaturized devices, and the arrival of the 5G era brings higher requirements for electromagnetic shielding and heat dissipation, and promotes the future process upgrade of electromagnetic shielding and heat conduction devices. The attenuation of electromagnetic shielding by electromagnetic shielding is mainly based on the principle of reflection and absorption of electromagnetic waves. Due to its excellent electrical conductivity, MXenes have recently gained increasing interest as highly efficient electromagnetic interference (EMI) and thermal management materials [20–23]. In fact, a typical EMI shielding material convert most of the EM radiation into heat dissipation [24,25], which can produce considerable heat accumulation. Therefore, combined materials for EMI shielding and thermal management are getting increasing attention [26]. While MXene shows promising results, currently is most used as a functional filler which can increase the electrical conductivity, and thus, the EMI shielding efficiency. MXene is therefore employed as a functional filler for different polymer matrix materials such as PEG [24], PEG-based polyurethane [27] or paraffin wax [28]. In addition, some innovative strategies are currently being pursued to improve electromagnetic shielding, such as studying the partial aggregation of the reinforcements in the polymer matrix [29], the migration mechanism of these reinforcements in the polymer blend and the viscosity of the blend [30], with the aim of creating a unique conductive network that can absorb more electromagnetic energy.

To sum up, in order to obtain a phase change material with excellent processability, high thermal conductivity, high phase change enthalpy, stable shape and leakage-proof, and electromagnetic shielding effect, we will use PLR as the support materials, PEG1k (melting temperature is close to 35 °C) and PEG6k (with melting temperature about 60 °C) as the phase change work substance and expect to prepare PCMs with tunable flexibility. The introduction of MXenes may take advantage of providing excellent multifunctional properties, including both electromagnetic shielding and thermal conductivity. In addition, the hydrophilicity of MXene itself will be beneficial to the ecofriendly mixing, compatibility and dispersion of materials to a certain extent. Generally speaking, the normal temperature of the mobile phone is between 30 and 50° when it is running. Because the above-mentioned phase transition temperature should be 30–50 °C, it is more appropriate to choose PEG 1k (with melting temperature around 35 °C). In addition, the introduction of PEG1k is expected to realize flexible and leak-resistant PCMs. PEG 6k or other PEG with a higher melting point are widely used in battery heat management [31,32], light-to-heat energy conversion and storage [33], energy efficiency of buildings [34], efficient thermal management of electronic components [35], and other applications. Therefore, in this work we will select PLR as the support material and MXene as the multifunctional filler to achieve excellent multifunctional PCMs with improved electromagnetic shielding and thermal conductivity. We will then demonstrate the practical application value of the phase change composites through temperature regulation of both mobile phones and solid-state drives.

2. Results and discussion

2.1. PCM preparation and structure investigation

The 2D layered MXene is synthesized through selectively etching the metal layers from the MAX precursor and newly incorporating some functional groups on the surfaces [36]. These terminating groups provide MXene sheets with hydrophilic surface and good solubility in an aqueous solution, which greatly facilitate the incorporation with water-soluble PLR/PEG in the following mixing procedure to prepare the multifunctional PCM composites [37].

In this work, the method for the preparation of MXenes employed in this work (Fig. 1a) is also detailed elsewhere [38,39]. The obtained SEM result of exfoliated MXene nanosheets is shown in Fig. 1b. The relevant XRD curve is given in Fig. S1. These results fully demonstrate the successful synthesis of MXene. The obtained MXene were blended to PLR/PEG to fabricate the PCM composites. After PLR, PEG and MXene are mixed and dried, the sample can be hot-pressed conveniently (Fig. 1f). The PLR-PEG1k relevant samples show excellent flexibility. Typically, the sample can be curled (Fig. 1e). As shown in Fig. 1d, large-area preparation can be achieved. In addition, PLR-1k-MX5, as a typical example, shows that it can be extruded in filament (Fig. 1g) and cut in granulation (Fig. 1h), which also demonstrates the possibility of continuous processing manufacturing and 3D printing to a certain extent.

Both cross-section morphologies of PLR-PEG1k (Fig. 1i) and PLR-1k-MX5 (Fig. 1j) are relatively rough, indicating that the fracture of the material is ductile fracture. Fig. 1k for sample PLR-6k shows the smooth fracture morphology. The introduction of MXene (PLR-1k-MX5) shows some cracks, which may be due to the spatial barrier of MXene nanosheets, inhibiting PEG from moving in a large range of space. On the other hand, MXene may induce the crystallization of PEG (the latent heat is improved based on DSC results). In addition, for both PLR-1k-MX5 and PLR-6k-MX5, there are no significant MXene aggregation in the large field of view (Fig. S2) and MXene can be tightly packed by the matrix, because no phase separation interface is detected. This shows that there is a good interfacial interaction between MXene and the matrix. We assign that this good dispersion is due to the surface multipolar functional groups of MXene, which ensure that MXene is easily dispersed in water and forms hydrogen bonds [20] with the matrix in PCM to obtain excellent dispersion, as illustrated in Fig. 1m. FTIR data (Fig. 1n) show that the introduction of MXene will weaken the hydrogen bond association (maybe among the –OH groups on cyclodextrin) to a certain extent, so the hydroxyl signal near 3400 cm^{-1} tends to be significantly weakened. The FTIR curves of all the samples are also provided in Figs. S4 and S5.

2.2. Phase change performances

The XRD curves of the typical samples are shown in Fig. 2a. The peak at 2θ∼9.8° corresponds to the crystalline (002) plane of MXene. The peak at 12.7° (110) obtained from the PLR crystal consisting of α-Cyclodextrin and PEG [40]. The peaks at ∼19° and ∼23° can be attributed to the crystal planes (120), (112)/(032) respectively, of PEG. The results showed that PLR/PEG (both 1k and 6k) maintained good crystallization ability with the introduction of MXene. This is also a prerequisite for the energy storage during phase change. In addition, the presence of PLR crystallization peaks ((002) plane) indicates the presence of physical crosslinking points for α-Cyclodextrin with Poly(ethylene oxide) (PEO) chain crystallization, which is an important reason for ensuring the excellent shape stability of the PCMs during phase transition under 70 °C, because the melting temperature of the α-Cyclodextrin with PEO chain

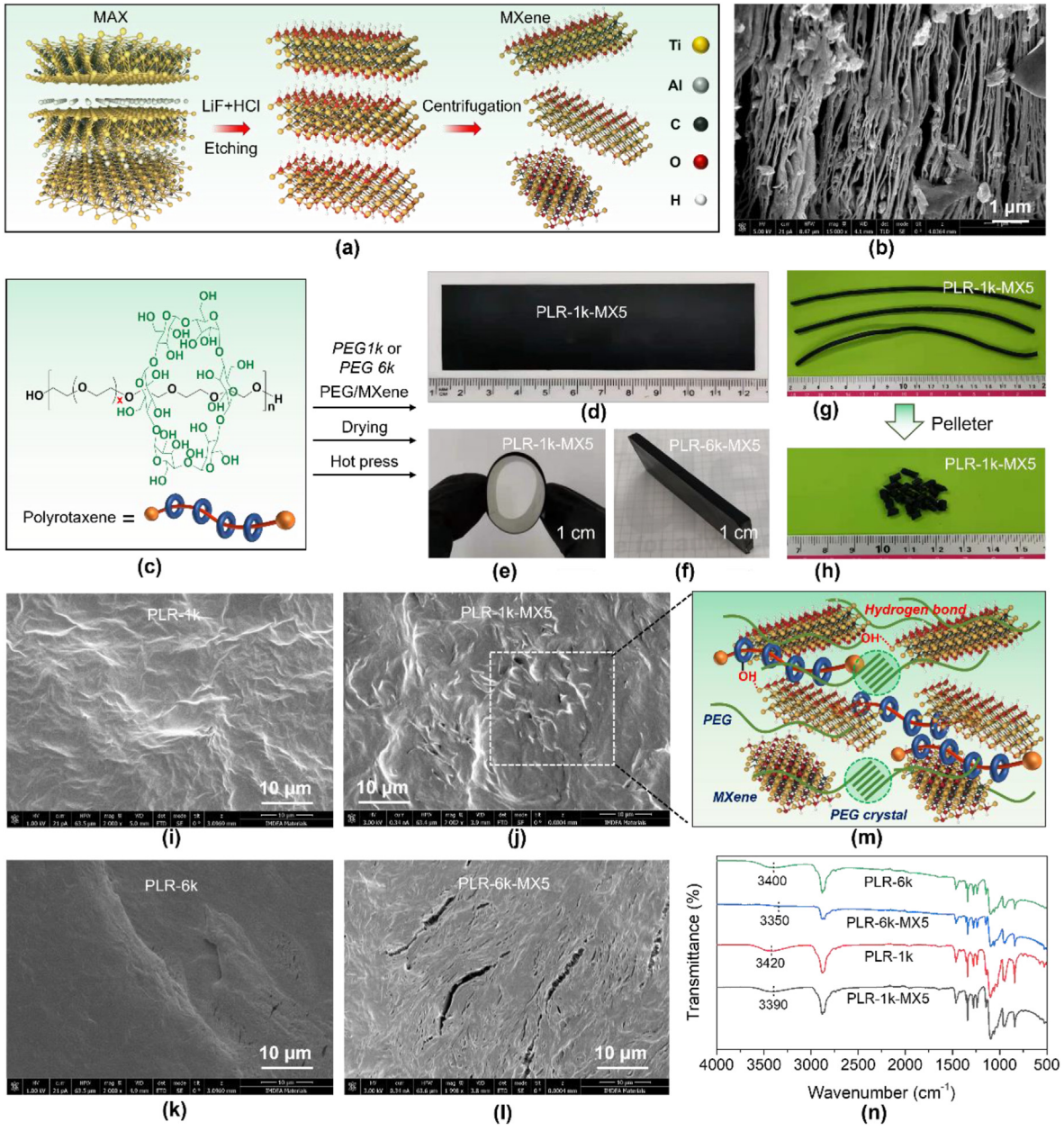

Fig. 1. (a) Two steps for fabrication of MXene from MAX-Ti_3AlC_2, (b) Scanning Electron Microscope (SEM) morphology of the obtained MXene nano sheets, (c) chemical structure of polyrotaxane (as support materials), (d) the PCM sheet with large size (11 cm in length, 4 cm in width and 0.5 mm in thickness), (e) image of sample PLR-1k-MX5 to show the flexibility, (f) sample PLR-6k-MX5 to show the re-mouldability (hot press from freeze dried foam), (g) filaments of sample PLR-1k-MX5 with diameter 4 mm, (h) pellets of sample PLR-1k-MX5 from the above filaments, (i) section morphology of PLR-1k, (j) section morphology of PLR-1k-MX5, (k) section morphology of PLR-6k, (l) section morphology of PLR-6k-MX5, (m) dispersion and interaction illustration of MXene in the PCM matrix, and (n) Fourier-transform infrared spectroscopy (FTIR) curves of typical samples: PLR-1k, PLR-1k-MX5, PLR-6k, and PLR-6k-MX5.

crystallization is higher than 90 °C [18].

PLR has been proven to be an excellent phase change material [11] and an excellent support material for PEG work substance. With the introduction of MXene in this study, the obtained samples still maintain excellent shape stability and anti-leakage properties. As shown in Fig. 2b, no significant dimensional changes or leakage occurred in the material after heat treatment at 70 °C for 2 h (on filter papers). We continue to conduct Differential scanning calorimetry (DSC) testing on the samples to collect their typical phase change performance parameters. The specific test curves are given in Figs. S6–S15 and relevant parameters are listed in Table S2. Fig. 2c and d shows the latent heat of phase change (ΔH_m) and crystallization enthalpies (Δ Hs). For the PEG 1k relevant samples, both Δ Hs and Δ Hm showed a downward tendency after the introduction of MXene. Fortunately, the latent heat of fusion can still be maintained at 123.9 J/g at 5 wt% of MXene. For the PEG 6k system, the terminal effect of PEG is lower than that of PEG 1k, the crystallization ability might be enhanced to a certain extent. The introduction of MXene may act as a crystallization-induced nucleation agent in such a situation, hence the enthalpy increase that occurs at low MXene loading (for both sample PLR-6k-MX1 and PLR-6k-MX3). When the MXene content increases to 5 wt%, the impurity effect of the fillers dominates and the enthalpy value decreases but still maintains a high level of 145.4 J/g for PLR-6k-MX5. Cycling stability (Both PLR-1k-MX5 and PLR-6k-MX5) was performed for 80 cycles. It can be seen that core indicators such as Δ Hm and Δ Hs remain relatively stable (Fig. 2e and f), which shows that the material has good cycle stability. The specific parameters are given in Tables S3 and S4.

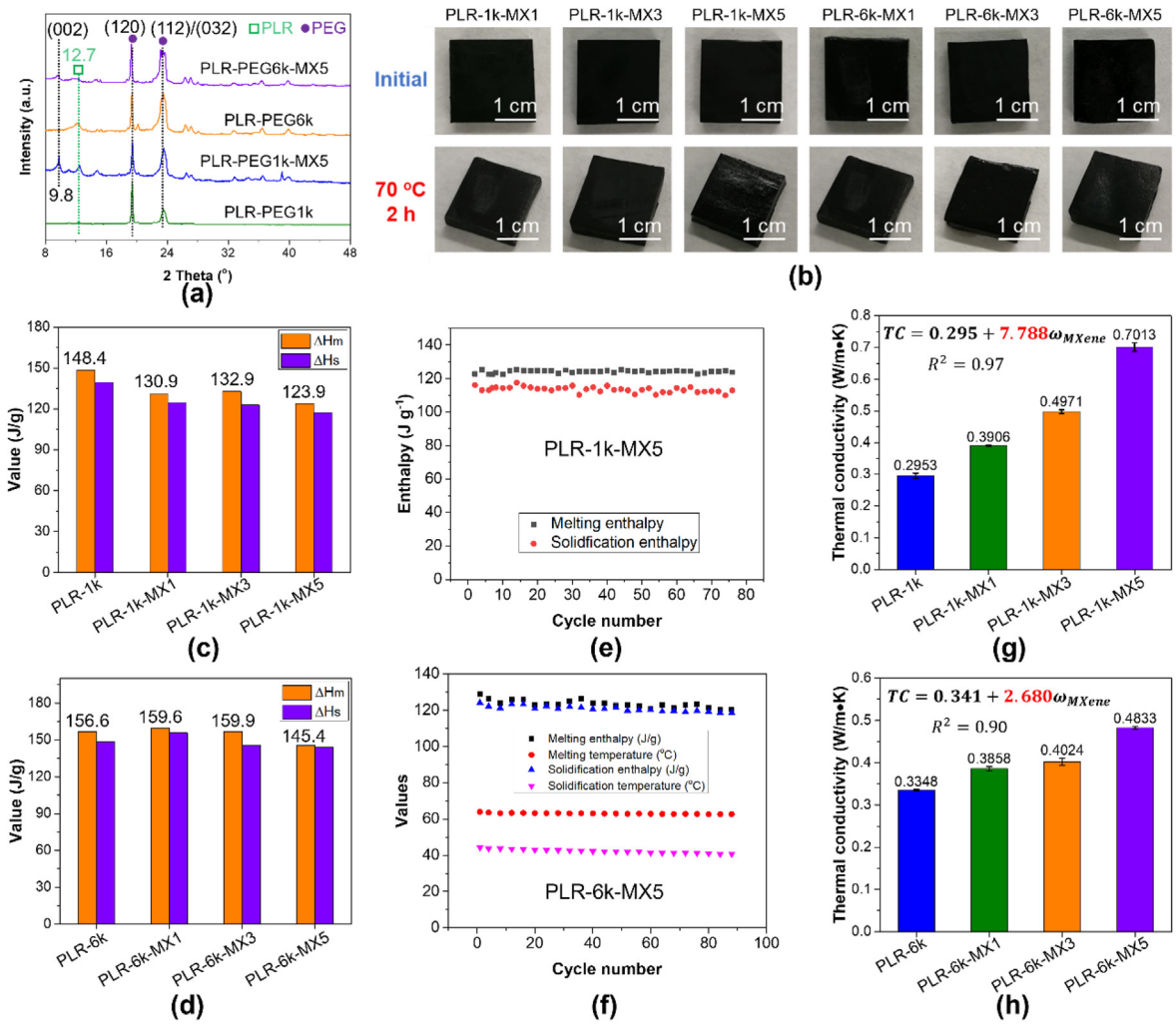

Fig. 2. (a) XRD curves of samples PLR-1k, PLR-1k-MX5, PLR-6k and PLR-6k-MX5, (b) Intuitive characterization of the anti-leakage performance and shape stability of the samples, (c) Melting enthalpy values and solidification enthalpy values of PLR-PEG 1k system, (d) Melting enthalpy values and solidification enthalpy values of PLR-PEG 6k system, (e) parameters of sample PLR-1k-MX5 for cycling stability, (f) parameters of sample PLR-6k-MX5 for cycling stability, (g) thermal conductivity results of PLR-PEG1k system, and (h) thermal conductivity results of PLR-PEG6k system.

Fig. 2g and h shows the Thermal Conductivity (TC) indexes of the samples. The TC increased with the increasing of MXene contents for both PEG 1k and PEG 6k relevant samples. Specifically, when 5 wt% of MXene is added, the PLR-1k relevant samples can increase from 0.2953 W/(m • K) to 0.7013 W/(m • K) (with an increase of 137.5 %); while the PLR-6k system can increase from 0.3348 W/(m • K) to 0.4833 W/(m • K) (with an increase of 44.3 %). As it further can be seen in Fig. 2g, and h, the PEG1k relevant samples show a higher increasing slope (7.788) than that of PEG 6k relevant samples (with value of 2.680). The possible reason is that MXene forms a better network structure in the PEG 1k system and acts as a thermally conductive framework. Some evidence can be obtained from the image after TGA and fire test, which will be further discussed in section 2.4. On the other hand, it can be seen from Scanning electron microscope (SEM) that PEG6k is spatially limited by 2D MXene, and its crystallinity is quite high relative to that of PEG 1k, so some void defects were generated during the cooling process (Fig. S3).

2.3. Electrical conductivity and electromagnetic shielding

EMI shielding is related to the electrical conductivity of the composites. Therefore, DC electrical conductivity is recorded and presented in Fig. 3a. Among the different PLR-PEG-MXene composites, it is observed that composites containing PEG 1k present a higher conductivity than those with PEG 6k s. Regarding MXene loading, conductivity increases with the increasing of MXene content [41]. Typically, the maximum conductivity is reached for PLR-1k-MX5 with $3.23 \cdot 10^{-6}$ S/m, compared to $1.36 \cdot 10^{-7}$ S/m of PEG 1k, which are in agreement with other reports [42].

To determine the EMI shielding mechanism of the samples, EMI SE was measured and is presented in Fig. 3b between the range of 1.8–6.0 GHz. The schematics of the experimental setup are shown in Fig. 3c. The results are in clear agreement with the conductivity results: higher conductive samples (samples which contain MXene) offer a higher EMI SE shielding, reaching a maximum of 4.67 dB at 5.6 GHz for the most conductive sample, PLR-1k-MX5. These results are in accordance with previous reports [24]. It has also been found that the total value of EMI shielding effectiveness in other reinforced polymers, with a constant MXene ratio, increases slightly with increasing frequency (Fig. 3b), which is also in agreement with previous findings mentioned in previous reports [43].

For far-field (Fig. 3b), it can be concluded that increasing the percentage of MXene generates an increase in the attenuation of the transmitted signal, but it is also observed that a higher MXene content generates a higher shielding, which is due to the fact that this usually results in a higher polymeric conductivity by reducing the mean free volume of the polymer [44]. Notably, the origin of the shielding, both in

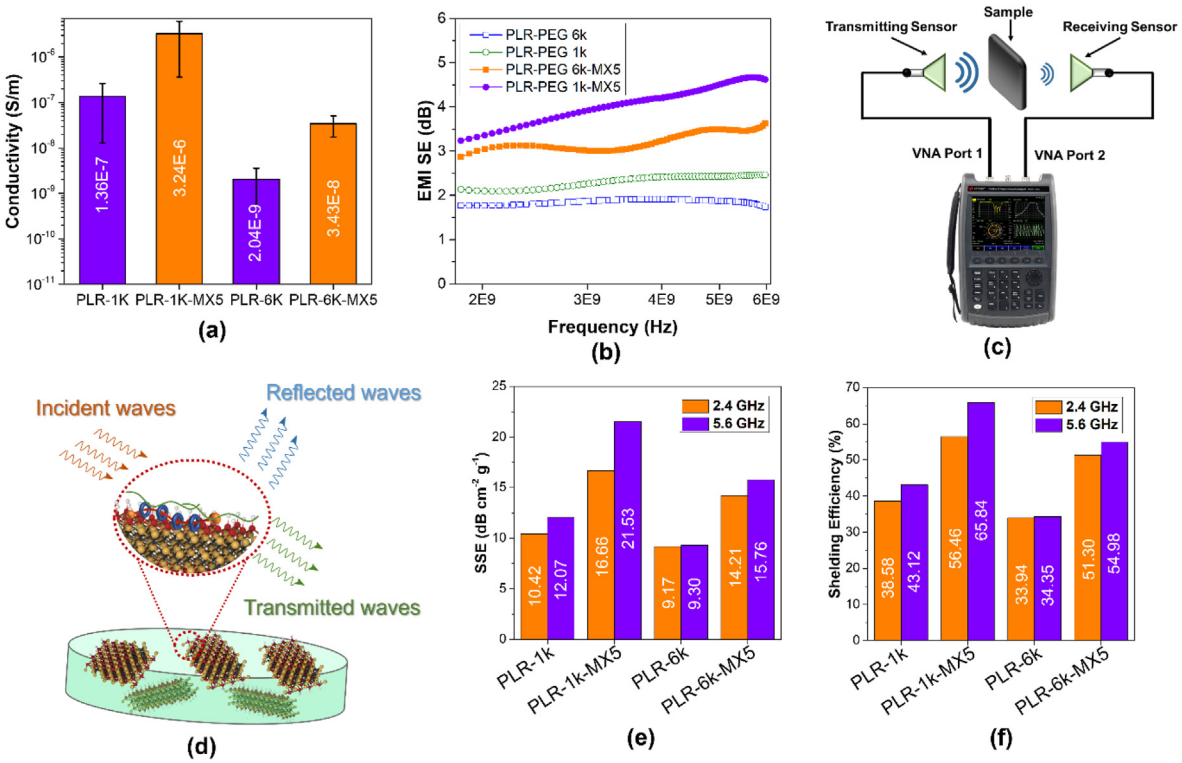

Fig. 3. (a) Electrical conductivity of PLR/PEG/MXene composites upon loading, (b) Electromagnetic Interference (EMI) Shielding Efficiency (SE) of the different samples with thickness of 1.5 mm, (c) shielding measurement test scheme, (d) schematic representation of the mechanism of EMI shielding of the PLR/PEG/MXene composites, (e) specific shielding effectiveness (SSE) and (f) shielding efficiency (SE).

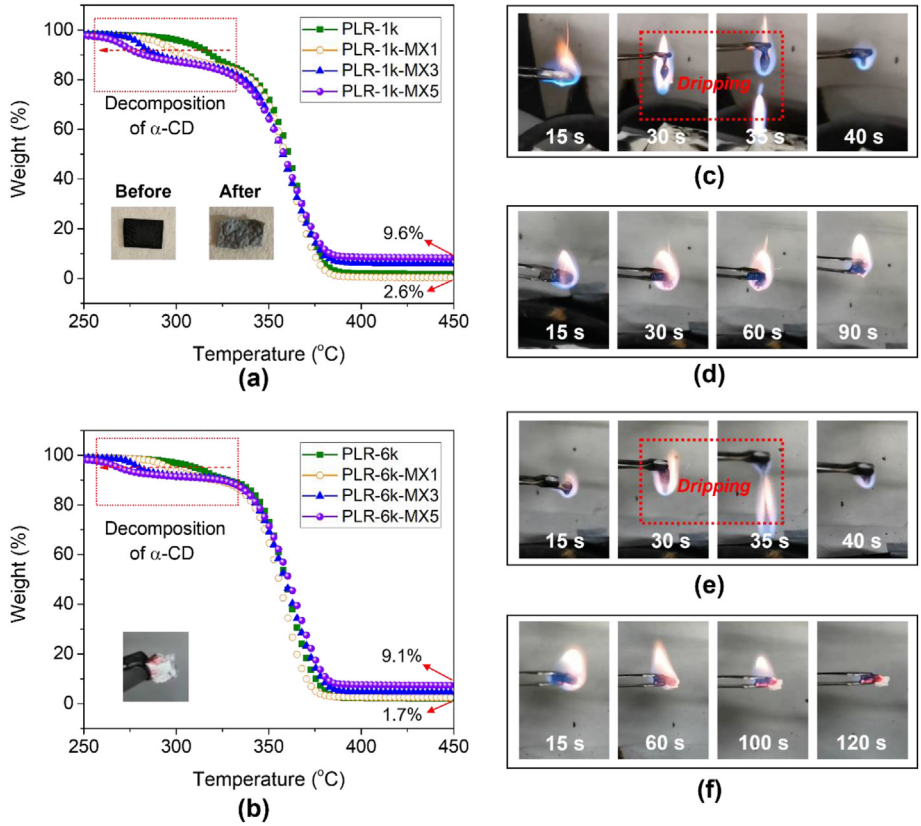

Fig. 4. (a) Thermogravimetric Analysis (TGA) curves of PEG1k relevant PCM composites, (b) TGA curves of PEG 6k relevant PCM composites, (c) fire behaviors of sample PLR-1k, (d) fire behaviors of sample PLR-1k-MX5, (e) fire behaviors of sample PLR-6k, and (f) fire behaviors of sample PLR-6k-MX5.

the near and far field, is caused by interface polarization, defective polarization and surface functional group polarization [45,46]. This explains why PLR-1k despite having a higher conductivity shows lower EMI shielding than PLR-6k-MX5. With respect to the near-field tests, PLR-PEG/MXene, as shown in the results (Figs. S16 and S17), can be useful for applications where it is desired to shield the electric fields completely and let the magnetic field pass through. Another application of great interest would be to take advantage of the interaction with the nearby electric fields, to generate photothermal conversion of the same, so that by harnessing this heat energy is generated [47].

A possible mechanism of the EMI shielding is depicted in Fig. 3d, where the incident electromagnetic waves interact with the PLR-PEG-MXene composite, being partially reflected, and partially absorbed by the sample. Due to the presence of local currents of the MXene, the incoming EM waves interact with the high-density electron carriers, which leads to massive ohmic losses and thus, attenuation of the EM wave [20]. Also, due to the reflections between multiple MXene nanosheets, the dissipation of the EM is promoted. This is the reason why higher loading implies higher EMI shielding. Nonetheless, part of the EMI radiation can pass through the sample, while due to the higher MXene content, as observed, lower EM waves can pass through.

The specific shielding effectiveness (SSE) and the shielding efficiency are depicted also in Fig. 3e and f for two representative frequencies at two wave bands, 2.4 GHz (S-band) and 5.6 GHz (C-Band), the latter parameter takes into consideration the density and the thickness of the samples, showing that the denser samples (those with PEG1k and MXene) show a higher SSE, even without the addition of MXene, which should be taken into consideration for low-weight applications.

2.4. Thermal stability and fire behaviors

As shown in Fig. 4a and b, we found that the introduction of MXene will catalyze the early decomposition of cyclodextrin, as shown in the red rectangle regions in both Fig. 4a and b, which directly manifests as the forward shift of the first step. Fortunately, all samples began to decompose above 250 °C, which fully ensures that the material is stable within the normal thermal management application temperature range. The residual content at 800 °C was improved by three times higher than that of neat PLR-PEG. We further conducted direct ignition experiments on samples PLR-1k, PLR-1k-MX5, PLR-6k and PLR-6k-MX5, and the corresponding pictures are shown in Fig. 4c and d. We discover that the layered MXene endowed PLR-PEG film with remarkable anti-dripping performance (Fig. 4c and e), and the layer structure of composite film remained during the whole combustion process (shown in Fig. 4d and f). The protective barrier of MXene can effectively blocked the transfer of heat/oxygen and then prevented the appearance of melt drip. In addition, the complete shape and structure of the textile can be maintained even after burning test (Fig. 4b inset). The well-distributed MXene nanosheets acted as the effective flame retardant on the PLR-PEG, which is proved in the previous reports [37].

2.5. Application cases

2.5.1. Thermal regulations of smart phone by using flexible PLR-PEG1k relevant PCMs

To demonstrate the applicability of the assembled PCMs, two case studies are presented. Firstly, as shown in the schematic diagram of Fig. 5a, the test process of PCM's thermal management during the use of a smartphone is evaluated. The PCM samples with a thickness of about 0.5 mm are covered on the Central Processing Unit (CPU) core area, which corresponds to the upper half of the mobile phone. We divide the PCMs into three temperature regions of specific concern, namely region A, B and C. The temperature changes during the use of WeChat video calls. The screenshot of the infrared imaging process of its specific test is shown in Fig. 5b. Compared with the reference sample (the test curves or images without PCM), the samples with PCM all show a better temperature adjustment. Typically, the CPU area temperature has a significant difference among the reference sample and the PCM containing samples at t = 3000 s. Based on the temperature changes in each temperature region, the specific temperature-time curves were derived. First, region A, which is the CPU area, is the initial heat source for investigation. Its thermal response is almost determined by the phase transition process because the sample thickness is low and is close to the core heat source.

All samples containing PCM have a significant effect of regulating temperature compared with reference and it can be further found that more MXene can ensure better thermal management capacity, especially

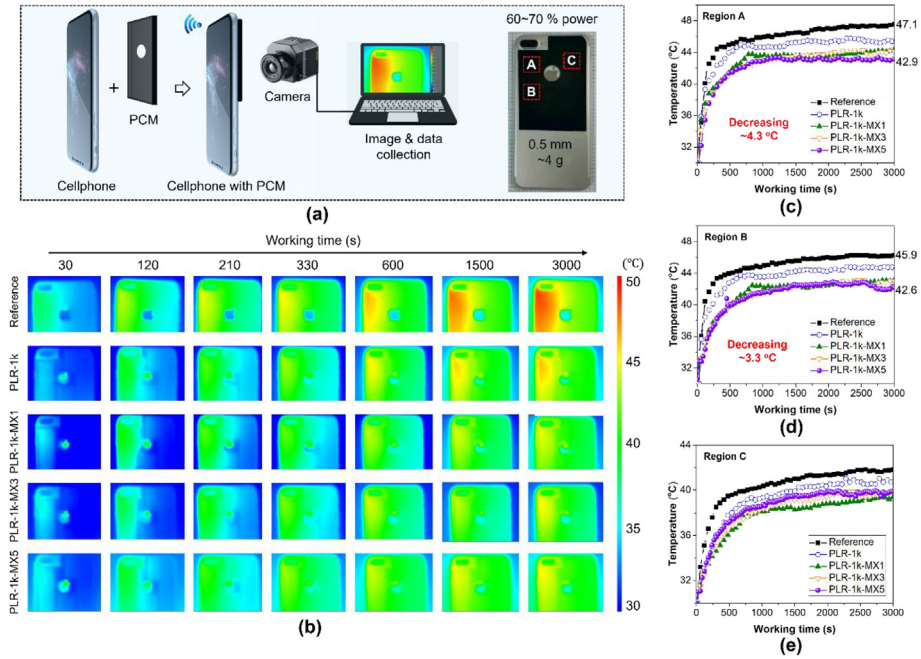

Fig. 5. (a) Phone with PCM and the temperature regulation illustration, (b) Infrared (IR) images of the samples: empty cellphone, PLR-1k, PLR-1k-MX1, PLR-1k-MX3 and PLR-1k-MX5, (c) temperature change curves of region A, (d) temperature change curves of region B and (e) temperature change curves of region C.

for region A. It is worth pointing out that sample PLR-1k-MX5 can decrease 4.3 °C of the reference temperature of region A. For region B, the heat source mainly comes from the absorption from region A, mainly because they are quite close. Therefore, its temperature change tendency is similar to that of region A. Since the temperature in Region C of cellphone is relatively low (comparing to Region A and B), its heat source is not only the one generated by the mobile phone, but also the heat transfer from Region A and B of the PCM sheet. A combination of factors results in a sample with high thermal conductivity having a high temperature at the same time (Fig. 5e). We can understand that for low thermal conductivity, PCM with high enthalpy value is conducive to the regulation of heat absorption and cooling. If PCM also has high thermal conductivity, it can also have the effect of equalizing heat. Because PLR-1k-MX5 has the highest thermal conductivity, its temperature increase in the middle and late stages significantly exceeds that of several other samples (Fig. 5e and f). It can be seen that the heating process of the overall components has a relatively long period of stability in the later stage. This is mainly because the heat absorption and heat dissipation of the material (through conduction and diffusion in the surrounding materials like air transmission) form a balance within a certain period of time.

2.5.2. Solid state disk (SSD) heat management

Another key application of PCMs is the thermal management of electronic devices. As shown in Fig. 6a, phase change materials usually work with metal heatsink to regulate the temperature of solid state disk (SSD). As shown in Fig. 6b, the insulation layer, protecting sheet (Polypropylene (PP) with 2 mm in thickness), PCM and the metal heatsink stacked together from the bottom to the top. Fig. 6c shows the schematic diagram and a top view photograph of two schematic devices with PCM of the whole material test system. Fig. 6d shows the IR images of different samples at different heating time. We can further obtain the measured temperature change heating curves, as shown in Fig. 6e and f.

As shown in Fig. 6e and f, the state of the device can be relatively stable after heating for 750 s. During the heating cycle, sample PLR-6k and PLR-6k-MX5 showed significantly better temperature control capacity than both the reference sample (without PCM protection) and commodities (3 M and JOSBO as examples). Specifically, the temperature of the protecting sheet with PCM was significantly lower (e.g. 69.0 for the sample with PLR-6k-MX5, showing a decreasing of 7.9 °C) than that of blank sample (76.9 °C at t = 3000 s) and commercial PCMs (74.8 °C at t = 3000 s for 3 M, 75.8 °C at t = 3000 s for JOSBP). The DSC curves of the commercial PCMs are given in Figs. S26 and S27. It can be found that the latent heat values of both commercial PCM are very low (2–4 J/g). Therefore, its thermal control mainly depends on its heat conduction to the heat sink to achieve heat dissipation. Although its thermal conductivity is generally higher than 1.5 W/(m·K). However, the results of this study show that under a certain time scale, the phase change enthalpy plays a significant role in the thermal management of electronic devices. The significant temperature difference for a long time fully shows the practical significance of PCM in the field of thermal control of electronic devices.

3. Conclusion

PLR/PEG/MXene nano-PCM composites with different PEG molecular weight (PEG 1k and PEG 6k) and various contents of MXene (1 %, 3 % and 5 wt%) were successfully prepared. The addition of MXene to PLR/

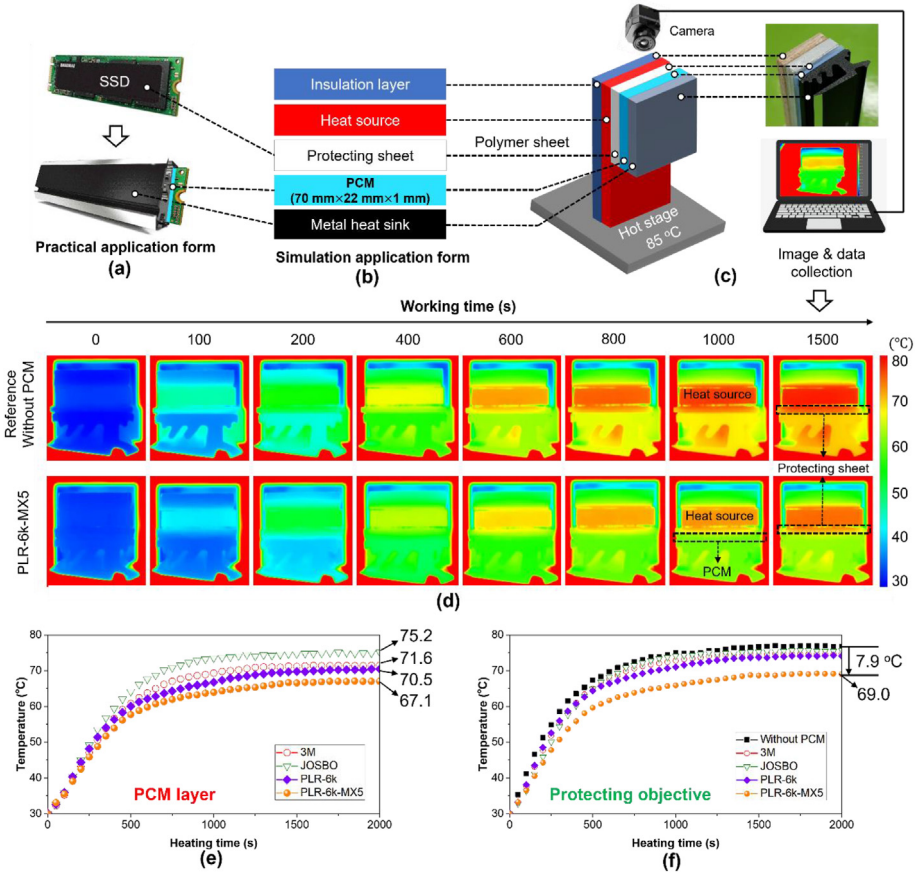

Fig. 6. (a) Solid state disk (SSD) and the image of SSD with heat sink; (b) Layered structure of simulated device; (c) the testing illustration and the images of the devices; (d) IR images of typical samples: the device without PCM and with PLR-6k-MX5; (e) the heating curves of the PCM in current work and some typical commercial samples; and (f) heating curves of the protecting sheet without PCM and with PCMs.

PEG maintained form stability and the heat storage capacities during phase transition. A high thermal performance was observed, obtaining high latent heat values (123.9–130.9 J/g for PLR-PEG 1k-MXene and 145.4–159.6 J/g for PLR-PEG 6k-MXene) and good cycle stability. The MXene contributed a significant increase of thermal conductivity with 44.3 % for PLR-1k-MX5, and 137.5 % for PLR-6k-MX5, compared to PLR-PEG in thermal conductivity, and the increase was linear with increasing MXene content. The introduction of MXene can significantly improve the electromagnetic shielding performance of PCM composites. Samples which contain MXene offer a higher EMI SE shielding, reaching a maximum of 4.67 dB at 5.6 GHz for the most conductive sample, PLR-1K-MX5. The introduction of MXene has a significant promotion effect on TGA residue, and there is no droplet formation during the combustion process. These results show that MXene has a certain flame-retardant function for the PLR-PEG phase change system. The application cases showed great heat regulation capacities for both smartphone and Solid State Disk, which combined with the higher EMI shielding performance that can be employed for protection of electronic devices.

CRediT authorship contribution statement

Guang-Zhong Yin: Conceptualization, Methodology, Data curation, Writing-original draft, Writing-review & editing, Supervision, Funding acquisition. **Alba Marta López:** Data curation, Methodology, Writing-review & editing. **Ignacio Collado:** Data curation, Writing-original draft, Writing-review & editing. **Antonio Vázquez-López:** Data curation, Writing-original draft, Writing-review & editing. **Xiang Ao:** Data curation, Writing-review & editing. **Jose Hobson:** Data curation,Writing-review & editing. **Silvia G. Prolongo:** Writing-review & editing, Funding acquisition. **De-Yi Wang:** Methodology, Writing-review & editing, Supervision, Funding acquisition.

Declaration of competing interest

The authors declare that they have no known competing financial interests or personal relationships that could have appeared to influence the work reported in this paper.

Acknowledgment

This work was supported by both BIOFIRESAFE (No.: PID2020-117274RB-I00) and NEWSAFE (No.: PID2022-143324NA-I00) Projects funded by Ministerio De Ciencia E Innovación (MINECO, Spain). This work was also partially supported by the Agencia Estatal de Investigación of Spanish Government [PROJECTS TED2021-131102B-C21 and PID2022-138496OB-I00].

Appendix A. Supplementary data

Supplementary data to this article can be found online at https://doi.org/10.1016/j.nanoms.2023.12.004.

References

[1] Y.-J. Yim, J.J. Lee, A. Tugirumubano, S.H. Go, L.K. Kim HGKwac, Electromagnetic interference shielding behavior of magnetic carbon fibers prepared by electroless FeCoNi-plating, Materials 14 (14) (2021) 3774.
[2] S. Sundararajan, P.S. Samui ABKulkarni, Versatility of polyethylene glycol (PEG) in designing solid–solid phase change materials (PCMs) for thermal management and their application to innovative technologies, J. Mater. Chem. A 5 (35) (2017) 18379–18396.
[3] F. Souayfane, P.-H. Fardoun Fbiwole, Phase change materials (PCM) for cooling applications in buildings: a review, Energy Build. 129 (2016) 396–431.
[4] F.S. Javadi, P. Metselaar Hscganesan, Performance improvement of solar thermal systems integrated with phase change materials (PCM), a review, Sol. Energy 206 (2020) 330–352.
[5] S. Gharbi, S.B. Harmand Sjabrallah, Experimental comparison between different configurations of PCM based heat sinks for cooling electronic components, Appl. Therm. Eng. 87 (2015) 454–462.
[6] E. Sarier Nonder, Organic phase change materials and their textile applications: an overview, Thermochim. Acta 540 (2012) 7–60.
[7] Jing J, Liu Hwang X, Long-term infrared stealth by sandwich-like phase-change composites at elevated temperatures via synergistic emissivity and thermal regulation. Adv. Funct. Mater. n/a (n/a): 2309269.
[8] W. Aftab, X. Huang, W. Wu, Z. Liang, R. Mahmood Azou, Nanoconfined phase change materials for thermal energy applications, Energy Environ. Sci. 11 (6) (2018) 1392–1424.
[9] G.-Z. Yin, X.-M. Yang, A.M. López, X. Ao, M.-T. Wang, J.G. Molleja, D.-Y. Wang, PLA aerogel as a universal support for the typical organic phase change energy storage materials, J. Energy Storage 73 (2023) 108869.
[10] G.-Z. Yin, X.-M. Yang, A.M. López, M.-T. Wang, W. Ye, B. Xu, D.-Y. Wang, Sodium alginate and Chitosan aided design of form-stable Polyrotaxane based phase change materials with ultra-high latent heat, Int. J. Biol. Macromol. 222 (2022) 429–437.
[11] G.-Z. Yin, J. Hobson, D.-Y. Duan Ywang, Polyrotaxane: new generation of sustainable, ultra-flexible, form-stable and smart phase change materials, Energy Storage Mater. 40 (2021) 347–357.
[12] R. Chen, R. Yao, R. Xia Wzou, Electro/photo to heat conversion system based on polyurethane embedded graphite foam, Appl. Energy 152 (2015) 183–188.
[13] P. Yuan, P. Zhang, S. Liang Tzhai, Effects of surface functionalization on thermal and mechanical properties of graphene/polyethylene glycol composite phase change materials, Appl. Surf. Sci. 485 (2019) 402–412.
[14] Y. Jiang, Z. Wang, M. Shang, S. Zhang Zzhang, Heat collection and supply of interconnected netlike graphene/polyethyleneglycol composites for thermoelectric devices, Nanoscale 7 (25) (2015) 10950–10953.
[15] S. Sundararajan, P.S. Samui ABKulkarni, Interpenetrating phase change polymer networks based on crosslinked polyethylene glycol and poly(hydroxyethyl methacrylate), Sol. Energy Mater. Sol. Cell. 149 (2016) 266–274.
[16] G.-Z. Yin, X.-M. Yang, J. Hobson, D.-Y. López Amwang, Bio-based poly (glycerol-itaconic acid)/PEG/APP as form stable and flame-retardant phase change materials, Compos. Commun. 30 (2022) 101057.
[17] A. Kim, N.A. Wert, R. Gowd Ebpatel, Recent progress in PEG-based composite phase change materials, Polym. Rev. (2023) 1–52.
[18] G.-Z. Yin, A. Marta López, X.-M. Yang, X. Ao, D.-Y. Hobson Jwang, Polyrotaxane based leakage-proof and injectable phase change materials with high melting enthalpy and adjustable transition temperature, Chem. Eng. J. 444 (2022) 136421.
[19] F. Bétermier, N. Daher, L.A. Blanquer, J. Brun, A. Marcellan, N. Jarroux, J.-M. Tarascon, Understanding the electrochemical performances of Si anodes incorporating mechanically interlocked binders prepared from α-cyclodextrin-based polyrotaxanes, Chem. Mater. 35 (3) (2023) 937–947.
[20] Z. Ma, S. Kang, J. Ma, L. Shao, Y. Zhang, C. Liu, A. Wei, X. Xiang, L. Wei, J. Gu, Ultraflexible and mechanically strong double-layered aramid nanofiber–Ti3C2Tx MXene/silver nanowire nanocomposite papers for high-performance electromagnetic interference shielding, ACS Nano 14 (7) (2020) 8368–8382.
[21] Z.-D. Zhang, X.-F. Zhao, Q.-C. Zhang, J. Liang, H.-N. Zhang, T.-S. Zhang, C.-Y. Xue, Fully sprayed MXene-based high-performance flexible piezoresistive sensor for image recognition, Nano Materials Science (2023). https://doi.org/10.1016/j.nanoms.2023.06.001.
[22] Y.-Q. Mao, G.-H. Dong, W.-B. Zhu, Y.-Q. Li, S.-Y. Huang Pfu, Novel sandwich structured glass fiber Cloth/Poly(ethylene oxide)-MXene composite electrolyte, Nano Materials Science (2023). https://doi.org/10.1016/j.nanoms.2023.01.001.
[23] Q. Wang, N. Han, Z. Shen, X. Li, Z. Chen, Y. Cao, W. Si, F. Wang, B.-J. Ni, V.K. Thakur, MXene-based electrochemical (bio) sensors for sustainable applications: roadmap for future advanced materials, Nano Materials Science 5 (1) (2023) 39–52.
[24] H. Liu, R. Fu, X. Su, B. Wu, H. Wang, Y. Xu, X. Liu, MXene confined in shape-stabilized phase change material combining enhanced electromagnetic interference shielding and thermal management capability, Compos. Sci. Technol. 210 (2021) 108835.
[25] P. Song, B. Liu, H. Qiu, X. Shi, J. Cao Dgu, MXenes for polymer matrix electromagnetic interference shielding composites: a review, Compos. Commun. 24 (2021) 100653.
[26] Y.-K. Li, W.-J. Li, Z.-X. Wang, P.-Y. Du, L. Xu, L.-C. Jia, D.-X. Yan, High-efficiency electromagnetic interference shielding and thermal management of high-graphene nanoplate-loaded composites enabled by polymer-infiltrated technique, Carbon 211 (2023) 118096.
[27] X. Du, J. Xu, S. Deng, Z. Du, H. Cheng Xwang, Amino-functionalized single-walled carbon nanotubes-integrated polyurethane phase change composites with superior photothermal conversion efficiency and thermal conductivity, ACS Sustain. Chem. Eng. 7 (21) (2019) 17682–17690.
[28] V.A. Bose Pamirtham, A review on thermal conductivity enhancement of paraffinwax as latent heat energy storage material, Renew. Sustain. Energy Rev. 65 (2016) 81–100.
[29] J.-R. Tao, C.-L. Luo, M.-L. Huang, M. Weng Y-Xwang, Construction of unique conductive networks in carbon nanotubes/polymer composites via poly(ε-caprolactone) inducing partial aggregation of carbon nanotubes for microwave shielding enhancement, Compos. Appl. Sci. Manuf. 164 (2023) 107304.
[30] J.-R. Tao, D. Yang, Y. Yang, Q.-M. He, M. Fei Bwang, Migration mechanism of carbon nanotubes and matching viscosity-dependent morphology in Co-continuous Poly(lactic acid)/Poly(ε-caprolactone) blend: towards electromagnetic shielding enhancement, Polymer 252 (2022) 124963.
[31] W. Yang, R. Lin, X. Li, C. Li, Y. Wu, G. Zhang, X. Liu, S. Li, Y. Wang, High thermal conductive and anti-leakage composite phase change material with halloysite nanotube for battery thermal management system, J. Energy Storage 66 (2023) 107372.

[32] Y. Lu, R. Hu, Y. Chen Xbai, A strategy for constructing 3D ordered boron nitride aerogels-based thermally conductive phase change composites for battery thermal management, J. Mater. Sci. Technol. 160 (2023) 248–257.
[33] D. Yan, W. Ming, S. Liu, G. Yin, Y. Zhang, B. Tang, S. Zhang, Polyethylene glycol (PEG)/silicon dioxide grafted aminopropyl group and carboxylic multi-walled carbon nanotubes (SAM) composite as phase change material for light-to-heat energy conversion and storage, J. Energy Storage 36 (2021) 102428.
[34] A. Sarcinella, J.L. Barroso de Aguiar, M. Jesus Cfrigione, Thermal properties of PEG-based form-stable Phase Change Materials (PCMs) incorporated in mortars for energy efficiency of buildings, J. Energy Storage 67 (2023) 107545.
[35] P.P. Dutta, V. Saxena, S.K. Kumar Asahu, Investigation of finned heat sinks with PEG-6000/EG and PEG-6000/MWCNT composite phase change material for thermal management application, J. Energy Storage 70 (2023) 108057.
[36] R. Wang, W. Young Jang, W. Zhang, C. Venkata Reddy, R.R. Kakarla, C. Li, V.K. Gupta, J. Shim, T.M. Aminabhavi, Emerging two-dimensional (2D) MXene-based nanostructured materials: synthesis strategies, properties, and applications as efficient pseudo-supercapacitors, Chem. Eng. J. 472 (2023) 144913.
[37] W. Chen, P. Liu, Z. Liu Yliu, Recent advances in Two-dimensional Ti3C2Tx MXene for flame retardant polymer materials, Chem. Eng. J. 446 (2022) 137239.
[38] P. Zu, X. Xing, H. Wan, G. Yan Gzhang, Preparation of larger MXene layers and research progress in the field of gas adsorption and separation, Separ. Purif. Technol. 327 (2023) 125010.
[39] R. Kumar, S. Sahoo, J.-J. Joanni Eshim, Cutting edge composite materials based on MXenes: synthesis and electromagnetic interference shielding applications, Compos. B Eng. 264 (2023) 110874.
[40] S. Uenuma, R. Maeda, K. Yokoyama Hito, Formation of isolated pseudo-polyrotaxane nanosheet consisting of α-cyclodextrin and poly(ethylene glycol), Macromolecules 52 (10) (2019) 3881–3887.
[41] M. Han, C.E. Shuck, R. Rakhmanov, D. Parchment, B. Anasori, C.M. Koo, G. Friedman, Y. Gogotsi, Beyond Ti3C2Tx: MXenes for electromagnetic interference shielding, ACS Nano 14 (4) (2020) 5008–5016.
[42] X. Lu, H. Huang, X. Zhang, P. Lin, J. Huang, X. Sheng, L. Zhang, J-p Qu, Novel light-driven and electro-driven polyethylene glycol/two-dimensional MXene form-stable phase change material with enhanced thermal conductivity and electrical conductivity for thermal energy storage, Compos. B Eng. 177 (2019) 107372.
[43] S.-Y. Liao, X.-Y. Wang, X.-M. Li, Y.-J. Wan, T. Zhao, Y.-G. Hu, P.-L. Zhu, R. Sun, C.-P. Wong, Flexible liquid metal/cellulose nanofiber composites film with excellent thermal reliability for highly efficient and broadband EMI shielding, Chem. Eng. J. 422 (2021) 129962.
[44] D. Pei, Z. Wang, Z. Peng, J. Zhang, Y. Deng, Y. Han, L. Ye, Y. Geng, Impact of molecular weight on the mechanical and electrical properties of a high-mobility diketopyrrolopyrrole-based conjugated polymer, Macromolecules 53 (11) (2020) 4490–4500.
[45] P. He, M.-J. Zheng, Q. Liu, Z.-Y. Liu, R.-Z. Zuo, W.-Q. Cao, J. Yuan, M.-S. Cao, MXene nanohybrids: excellent electromagnetic properties for absorbing electromagnetic waves, Ceram. Int. 48 (2) (2022) 1484–1493.
[46] Z. Zeng, C. Wang, G. Siqueira, D. Han, A. Huch, S. Abdolhosseinzadeh, J. Heier, F. Nüesch, C. Zhang, G. Nyström, Nanocellulose-MXene biomimetic aerogels with orientation-tunable electromagnetic interference shielding performance, Adv. Sci. 7 (15) (2020) 2000979.
[47] M. Tang Xzhou, MXene-based electromagnetic wave response, J. Phys.: Energy 3 (4) (2021) 042001.